

DSR-Diff: Depth Map Super-Resolution with Diffusion Model

Yuan Shi, Bin Xia, Rui Zhu, Qingmin Liao, and Wenming Yang

Abstract—Color-guided depth map super-resolution (CDSR) improve the spatial resolution of a low-quality depth map with the corresponding high-quality color map, benefiting various applications such as 3D reconstruction, virtual reality, and augmented reality. While conventional CDSR methods typically rely on convolutional neural networks or transformers, diffusion models (DMs) have demonstrated notable effectiveness in high-level vision tasks. In this work, we present a novel CDSR paradigm that utilizes a diffusion model within the latent space to generate guidance for depth map super-resolution. The proposed method comprises a guidance generation network (GGN), a depth map super-resolution network (DSRN), and a guidance recovery network (GRN). The GGN is specifically designed to generate the guidance while managing its compactness. Additionally, we integrate a simple but effective feature fusion module and a transformer-style feature extraction module into the DSRN, enabling it to leverage guided priors in the extraction, fusion, and reconstruction of multi-model images. Taking into account both accuracy and efficiency, our proposed method has shown superior performance in extensive experiments when compared to state-of-the-art methods. Our codes will be made available at <https://github.com/shiyuan7/DSR-Diff>.

Index Terms—Diffusion model, guided depth super-resolution, feature fusion, image reconstruction

I. INTRODUCTION

DEPTH information is a crucial element in understanding three-dimensional spaces, complementing color data and playing a pivotal role in various computer vision applications, such as 3D reconstruction [1], SLAM [2] and semantic segmentation [3]. However, the practical use of modern depth sensors in consumer devices faces limitations due to budget and low-power constraints, resulting in significantly lower resolutions compared to their RGB counterparts. For example, the resolution of depth and color maps acquired by Kinect v2 is 512×424 pixels and 1920×1080 pixels, respectively. This resolution disparity hinders the effectiveness of the depth modality.

Considering the accessibility of high-resolution color images, various methods in color-guided depth super-resolution have emerged to harness both color and depth information.

This work was supported by the National Natural Science Foundation of China (Nos.62171251&62311530100) and the Special Foundation for the Development of Strategic Emerging Industries of Shenzhen (JCYJ20200109143010272). (Corresponding author: Wenming Yang.)

Y. Shi, B. Xia, Q. Liao and W. Yang are with the Shenzhen International Graduate School, Tsinghua University, Shenzhen 518055, China (e-mail: shiy22@mails.tsinghua.edu.cn; zjbixia@gmail.com; liaoqm@tsinghua.edu.cn; yang.wenming@sz.tsinghua.edu.cn).

R. Zhu is with Bayes Business School, City, University of London, London EC1V 0HB, United Kingdom (e-mail: rui.zhu@city.ac.uk).

Existing CDSR methodologies fall into three main categories: filtering-based methods, optimization-based methods, and learning-based methods. Filtering-based methods pose a risk of introducing artifacts, as they may inadvertently transfer the texture of the guidance image to the depth map. Meanwhile, optimization-based methods [4], [5] often involve time-intensive processes and may not yield satisfactory results when employing manually designed objective functions.

Learning-based methods, which acquire the mapping between low-resolution (LR) and precise high-resolution (HR) depth maps, have been proposed to address the limitations of hand-designed objective functions and filters [6], [7]. Being at the forefront of employing a learning-based method to tackle the challenges posed by the CDSR problem, MSG-Net [8] utilizes a CNN structure and employs multi-scale depth and color feature maps to enhance both the structure and texture of the HR depth maps. To leverage the edge information of the color maps, Wang et al. [9] proposed a two-stage method consisting of an edge-aware learning framework and depth restoration modules. Then, JIIF [10] was proposed to learn the interpolation weights, informed by the graph attention mechanism and implicit neural representation. Utilizing an efficient CNN architecture, AHMF [11] introduced an attention-based fusion mechanism for the integration of guidance information.

While learning-based methodologies have shown significant efficacy, the performance of these models is ultimately limited by the inherent capabilities of foundational models like CNN or Transformer. Recently, diffusion models have exhibited pronounced effectiveness in tasks encompassing both the synthesis [12], [13] and restoration [14], [15] of images. Diffusion models can iteratively generate high-quality images from Gaussian white noise. In comparison to CNNs and transformers, diffusion models exhibit stronger data fitting capabilities.

Nevertheless, the utilization of diffusion models for depth map super-resolution is confronted with a series of impediments. Firstly, the intrinsic iterative nature of diffusion models results in a temporal protraction. Secondly, the potent generative capability of diffusion models can lead to artifacts. To address these issues, we adopt a two-stage training approach and implement diffusion models in latent space, drawing inspiration from [15], to circumvent the need for recovering the entire image in CDSR problem. Specifically, in the first stage, we compress the ground truth depth map, color image and low-resolution depth map to generate a guiding prior using the proposed Guidance Generation Network (GGN).

arXiv:2311.09919v1 [cs.CV] 16 Nov 2023

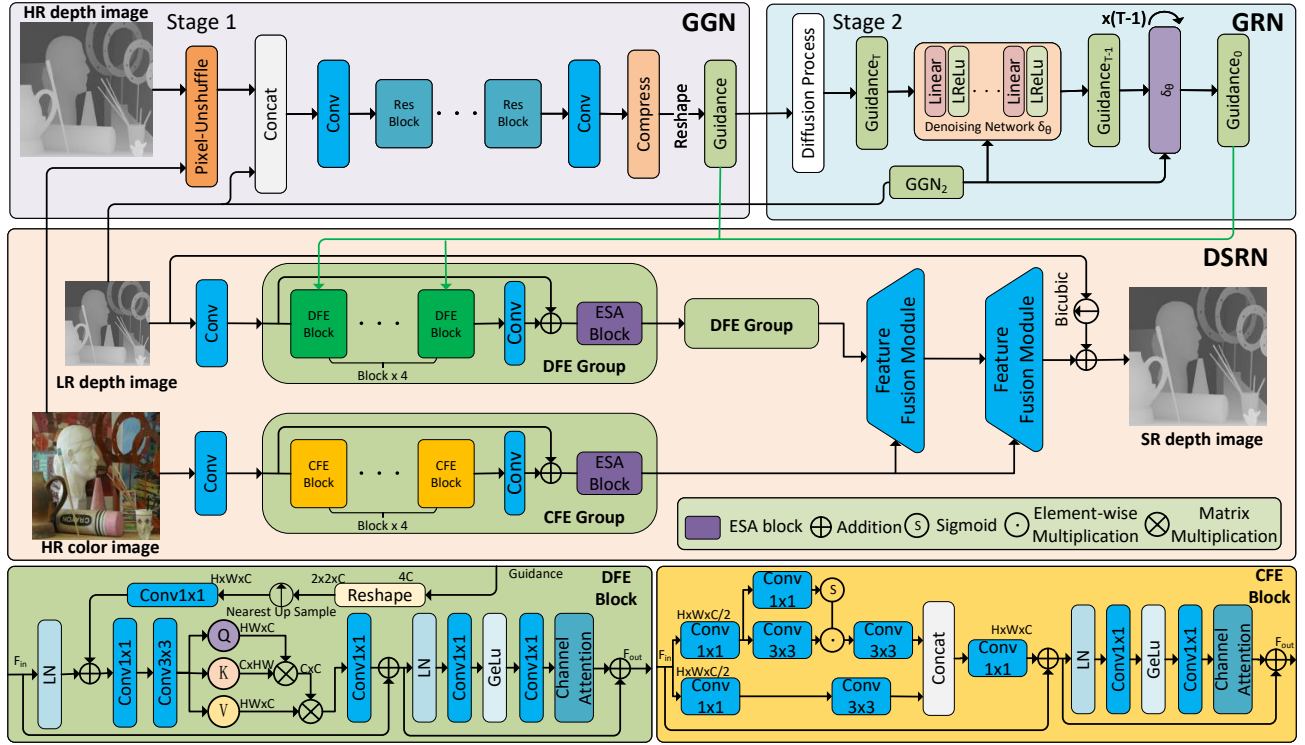


Fig. 1. The architecture of the proposed DSR-Diff. (a) DSRN utilizes two branches to extract features from LR depth images and HR color images, followed by feature fusion and reconstruction of the depth map, respectively. (b) In the first stage, LR depth images, HR depth images, and HR color images are input into GGN to generate guidance, directing the feature extraction and reconstruction in DSRN. (c) In the second stage, GRN is designed to estimate the guidance generated by GGN, thanks to the powerful estimation abilities of the diffusion model.

And an effective and efficient depth map super-resolution network (DSRN) is designed to utilize the guiding prior and reconstruct the depth map. Then the guiding prior is generated by guidance recovery network (GRN) with low-resolution depth map, relying on the powerful generative capability of diffusion models. Generally, the main contributions of our work are made as follows:

- We present a novel method, DSR-Diff, as the pioneering effort in applying diffusion models in latent space to enhance the resolution of depth maps, yielding noteworthy results.
- We devised the GGN to systematically generate compressed guiding priors. To fully harness these guiding priors, we introduced the DSRN, which integrates a guidance embedding module with our proposed simple yet efficient feature fusion module.
- Extensive experiments show that our proposed method achieves state-of-the-art performance, considering both precision and efficiency.

II. PROPOSED METHOD

A. Overview

Figure 1 shows our overall network architecture. We train DSR-Diff in two stages. In the proposed framework, DSRN functions as the main restoration network, employing LR depth images, HR color images, and guidance as inputs to reconstruct SR depth images. During the first stage, GGN generates guidance by extracting and compressing valuable features from HR color images, HR depth images, and LR

depth images. In the second stage, GRN generates guidance. In the forward process, the diffusion model progressively introduces noise into the guidance produced in the first stage. During the reverse process, the diffusion model utilizes LR depth images to estimate the necessary guidance.

B. Guidance Generation Network (GGN)

To provide accurate and concise guidance for DSRN, GGN is designed to extract essential information from HR depth images, HR color images, and LR depth images in the first stage of training. HR depth and color images are initially downsampled using pixel-unshuffle according to the scale factor. Subsequently, the downsampled images and LR depth images are concatenated and passed through several resblocks to generate guidance information. The feature maps of each channel in the guidance are divided into $K \times K$ blocks, and then we employ an operation similar to pooling to compress the information within these blocks. Given a concatenated feature $G \in \mathbb{R}^{H \times W \times C}$, the compressed guidance is $\hat{G} \in \mathbb{R}^{K^2 \times C}$. We set $K = 2$ in this problem.

C. Guidance Recovery Network (GRN)

In the second stage, we use GRN to generate guidance from the LR depth image. Guidance $G \in \mathbb{R}^{K^2 \times C}$ is initially generated by the GGN trained in the first stage. And we apply the diffusion process on G to sample G_T , which can be described as:

$$q(G_T|G) = \mathcal{N}(G_T; \sqrt{\bar{\alpha}_T}G, (1 - \bar{\alpha}_T)\mathcal{I}), \quad (1)$$

where T is the total number of iterations, $\mathcal{N}(\cdot)$ denotes the Gaussian distribution.

Since the guidance required for DSRN is very simple and compact, we can use a straightforward denoising network to estimate noise, making the guidance estimation simple and efficient. We start from T_{th} time step and run denoising iterations to obtain the estimated G_0 and send it to DSRN for joint optimization, which can be formulated as:

$$\hat{G}_{t-1} = \frac{1}{\sqrt{\alpha_t}} (\hat{G}_t - \epsilon \frac{1 - \alpha_t}{\sqrt{1 - \alpha_t}}), \quad (2)$$

where ϵ is the same noise. And in the reverse process, the LR depth images are initially input into GGN_2 , which has the almost same architecture with GGN except for the input, to generate the condition C_G . Then C_G , G_t and t are input to the denoising network δ_θ to estimate noise. After T times iterations, we get the estimated guidance $G_0 \in \mathbb{R}^{K^2C}$.

D. Depth Map Super-Resolution Network(DSRN)

DSRN can utilize the guidance generated by GGN or GRN to guide the feature extraction of depth images and obtain the reconstructed SR depth maps. DSRN primarily consists of the depth image feature extraction group (DFE group), the color image feature extraction group (CFE group), and the feature fusion module. In our pursuit of reconstructing depth images with a focus on both efficiency and accuracy, we opt for the utilization of two DFE groups to process depth features, alongside a dedicated CFE group specifically designed for handling color features.

By concatenating multiple DFE Blocks and incorporating an Enhanced Spatial Attention (ESA) block [16] in a sequential manner, a feature extraction architecture, denoted as the DFE Group, is obtained. We devised the DFE block based on the transformer block in [17]. And to leverage the guidance, the input guidance is first reshaped, upsampled to match the size of the feature map, and then added to the feature map after a 1×1 convolution. Given an input feature $F_{in} \in \mathbb{R}^{H \times W \times C}$ and guidance $G \in \mathbb{R}^{K^2C}$, This process can be formulated as:

$$\hat{F} = Conv(Up(Reshape(G))) + LN(F_{in}), \quad (3)$$

where $\hat{F} \in \mathbb{R}^{H \times W \times C}$ is the guidance-adjusted feature map, $Reshape(\cdot)$ is the reshape operation and $Reshape(G) \in \mathbb{R}^{K \times K \times C}$, K is a hyperparameter that we can use to control the compactness of guidance, $UP(\cdot)$ is the nearest upsampling, $Conv(\cdot)$ refers to a convolution with a kernel size of 1, and $LN(\cdot)$ is the layer normalization.

The structure of the CFE Group is consistent with that of the DFE Group. Due to the fact that the color image feature extraction branch does not require parsing information from the guidance, to enhance the efficiency of the model, we employed a simpler approach to design the CFE block inspired by [18] as shown in figure 1.

The extracted deep features and color features are upsampled to the same size and then fused within the feature fusion module (FFM), as illustrated in figure 2. The reconstructed SR depth image is obtained after passing through two FFMs. Depth and color features are upsampled through grid sampling,

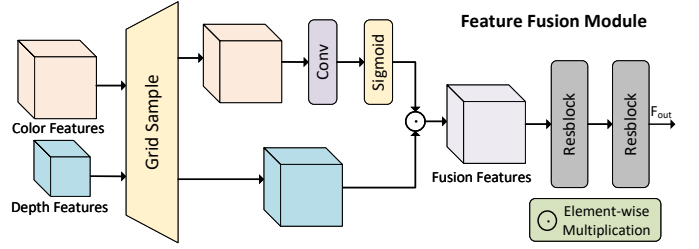


Fig. 2. The architecture of our proposed feature fusion module (FFM).

allowing the sampling of features at specific coordinates, thereby mitigating the impact of positional offsets in depth and color features.

Traditional learning-based DSR methods such as [10] and [8] often directly concatenate the color and depth features which tend to introduce unnecessary features in color image and require additional computation resources. In our proposed FFM, convolution is first applied to the complex color features, and then the upsampled color and depth features are directly multiplied together, which allows the effective components for reconstruction in both depth and color features to be retained, while weakening other non-essential features. Furthermore, two resblocks are concatenated at the end of the FFM for the refinement of the fused features.

E. Loss Function

In the first stage, our objective is to generate an effective guidance and get high-quality depth map through DSRN. So the training loss is defined as follows:

$$L_{img} = \|D_{GT} - D_{SR}\|_1 \quad (4)$$

where D_{GT} is the ground-truth depth image, D_{SR} is the reconstructed depth image, and $\|\cdot\|_1$ denotes the L_1 norm.

In the second stage, we need to estimate the guidance in the first stage and reconstruct the SR depth image. So we joint train the DRN and DSRN using loss function L_{com} :

$$L_{com} = \|G - G_0\|_1 + \|D_{GT} - D_{SR}\|_1 \quad (5)$$

And after training the model for a specified number of epochs, we still use L_{img} as the loss function for better reconstruction quality.

III. EXPERIMENTS

A. Implementation Details

1) *Dataset*: We select three benchmark RGB-D datasets, NYU V2 dataset [19], Middlebury dataset [20], [21], and Lu dataset [22], to evaluate our method. NYU V2 dataset includes 1449 RGB-D image pairs, with 1000 image pairs for training and the remaining 449 pairs for evaluation. Middlebury dataset and Lu dataset each have 30 and 6 RGB-D images pairs, respectively, all of which are utilized for evaluation.

TABLE I
 QUANTITATIVE COMPARISON WITH STATE-OF-THE-ART METHODS ON NYU V2, MIDDLEBURY, AND LU DATASETS IN TERMS OF RMSE (THE LOWER, THE BETTER). THE BEST PERFORMANCE IS SHOWN IN **BOLD**, WHILE THE SECOND BEST PERFORMANCE IS THE UNDERScoreD ONES.

Method	NYU V2			Middlebury			Lu		
	4×	8×	16×	4×	8×	16×	4×	8×	16×
Bicubic	4.28	7.14	11.58	2.28	3.98	6.37	2.42	4.54	7.38
MSG-Net [8]	3.02	5.38	9.17	1.88	3.45	6.28	2.30	4.17	7.22
DJF [23]	3.54	6.20	10.21	2.14	3.77	6.12	2.54	4.71	7.66
DG [24]	3.68	5.78	10.08	1.97	4.16	5.27	2.06	4.19	6.90
DJFR [25]	2.38	4.94	9.18	1.32	3.19	5.57	1.15	3.57	6.77
CUNet [26]	1.92	3.70	6.78	1.10	2.17	4.33	0.91	2.23	5.19
FDKN [27]	1.86	3.55	6.96	1.09	2.17	4.51	0.82	2.09	5.03
DKN [27]	1.62	3.26	6.51	1.23	2.12	4.24	0.96	2.16	5.11
DCTNet [28]	1.59	3.16	5.84	1.10	2.05	4.19	0.88	1.85	4.39
JiIF [10]	<u>1.37</u>	<u>2.76</u>	<u>5.27</u>	1.09	1.82	3.31	<u>0.85</u>	1.73	4.16
AHMF [11]	1.40	2.89	5.64	<u>1.07</u>	1.63	<u>3.14</u>	0.88	<u>1.66</u>	3.71
Ours	1.25	2.57	4.91	1.04	<u>1.67</u>	3.10	0.91	1.65	<u>3.92</u>

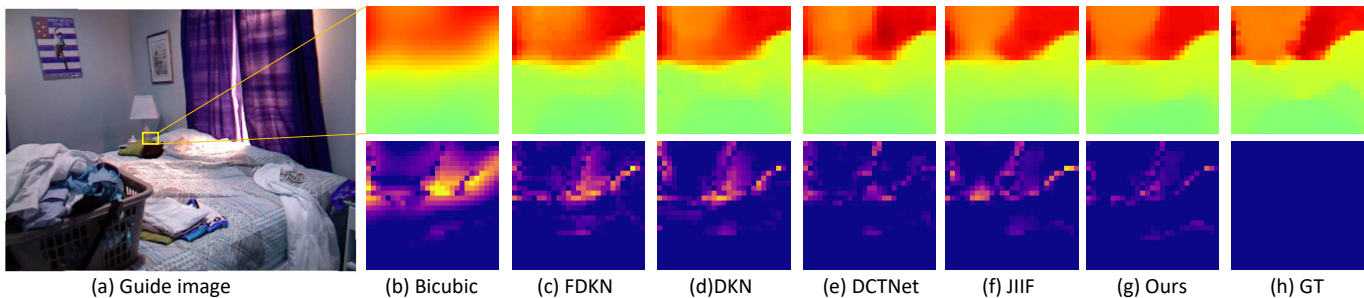


Fig. 3. Qualitative comparisons for x8 CDSR on the NYU v2 dataset. The first row is a zoomed-in view of the reconstructed depth map. The second row displays the error map between the results and the ground truth and brighter areas indicate more significant errors.

2) *Training Setting*: We apply a batch-mode learning method with a batch size of 1. Both the first and second stages require training for 300 epochs each. And The initial learning rate is set to 2×10^{-4} and decays by half every 80 epochs. The Adam optimizer with $\beta_1 = 0.9$, $\beta_2 = 0.99$ are used for optimization. In training the diffusion model, time step T are set to 4 and β_t ($\alpha_t = 1 - \beta_t$) linearly increase from 0.1 to 0.99. And all the experiments are performed with PyTorch on PC with one GTX 3090 GPU.

B. Comparisons with State-of-the-Art Methods

We compare DSR-Diff with state-of-the-art methods. Quantitative comparison results at scales of 4x, 8x, and 16x are presented in Table I. We use the average RMSE as the evaluation metric. Following [10], the average RMSE is measured in centimeters for the NYU v2 dataset. For the other two datasets, RMSE computations are carried out after scaling the depth values within the [0, 255] range.

The results in Table I clearly indicate that our proposed methods outperform alternative approaches in terms of accuracy. This superiority is particularly evident in the NYU v2 and Middlebury datasets, both of which include more test images. To further illustrate the superiority of our proposed method, we compared its runtime, parameters, and accuracy with the current state-of-the-art methods, as depicted in Figure 4. It

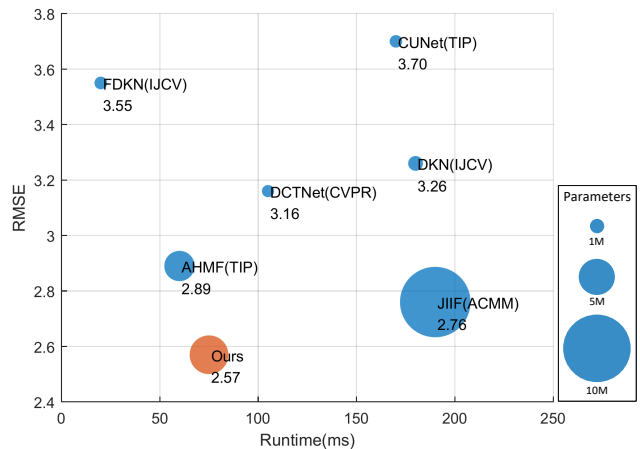


Fig. 4. Efficiency comparison with the current state-of-the-art methods for 8x CDSR on the NYU v2 dataset. The RMSE results are indicated below the name of each method, and the circular area serves as a visual representation of the model’s parameters.

is evident that, considering both efficiency and accuracy, our proposed method achieves state-of-the-art performance.

To better demonstrate the performance of DSR-Diff, we provide an intuitive visual comparison in Fig. 3. It can be clearly seen that the depth images reconstructed by DSR-Diff exhibit superior visual results, especially in areas with complex textures and edges.

C. Ablation Studies

To validate the effectiveness of each module in DSR-Diff, we conducted ablation experiments and the results are presented in Table II.

TABLE II
ABLATION STUDIES ON THE NYU V2 TEST SET

	M-1	M-2	M-3	M-4	M-5
GGN	×	×	✓	✓	✓
GRN	×	✓	×	✓	✓
FFM	✓	✓	✓	×	✓
Average RMSE	2.643	2.597	2.570	2.587	2.572

In M-1, the guidance is not incorporated into DSRN and we solely utilize the designed DSRN for depth image reconstruction. In M-2, the compress operation in GGN is replaced with a regular pooling operation. M-3 presents the results of the first stage. In conjunction with M-5, it substantiates the efficacy of the diffusion model in the second stage, aligning with the guidance generated by GGN. In M-4, the upsampled depth features and color features in FFM are directly concatenated together. The effectiveness of our proposed modules in enhancing the model’s performance is clearly evident.

IV. CONCLUSION

In this paper, we propose DSR-Diff, a guided super-resolution method with diffusion models. To address the time-consuming nature of diffusion models, we apply diffusion models in the latent space to generate compact guidance. Furthermore, we jointly optimize the diffusion model with an effective and efficient depth map super-resolution network (DSRN) to leverage the generated guidance. And a guidance generated network (GGN) is proposed to ensure that the guidance is appropriately generated and compressed. The feature fusion module (FFM) employs a simple yet efficient approach to achieve the integration of multi-modal features. Extensive experiments validate the effectiveness and superiority of our proposed DSR-Diff.

REFERENCES

- [1] J. Choe, S. Im, F. Rameau, M. Kang, and I. S. Kweon, “Volumefusion: Deep depth fusion for 3d scene reconstruction,” in *Proceedings of the IEEE/CVF International Conference on Computer Vision*, 2021, pp. 16 086–16 095.
- [2] K. Tateno, F. Tombari, I. Laina, and N. Navab, “Cnn-slam: Real-time dense monocular slam with learned depth prediction,” in *Proceedings of the IEEE conference on computer vision and pattern recognition*, 2017, pp. 6243–6252.
- [3] S. Weder, J. Schonberger, M. Pollefeys, and M. R. Oswald, “Routed-fusion: Learning real-time depth map fusion,” in *Proceedings of the IEEE/CVF Conference on Computer Vision and Pattern Recognition*, 2020, pp. 4887–4897.
- [4] Y. Zuo, Q. Wu, J. Zhang, and P. An, “Explicit edge inconsistency evaluation model for color-guided depth map enhancement,” *IEEE Transactions on Circuits and Systems for Video Technology*, vol. 28, no. 2, pp. 439–453, 2016.
- [5] W. Xu, Q. Zhu, and N. Qi, “Depth map super-resolution via joint local gradient and nonlocal structural regularizations,” *IEEE Transactions on Circuits and Systems for Video Technology*, vol. 32, no. 12, pp. 8297–8311, 2022.
- [6] Y. Zuo, Q. Wu, Y. Fang, P. An, L. Huang, and Z. Chen, “Multi-scale frequency reconstruction for guided depth map super-resolution via deep residual network,” *IEEE Transactions on Circuits and Systems for Video Technology*, vol. 30, no. 2, pp. 297–306, 2019.
- [7] Y. Zuo, Y. Fang, Y. Yang, X. Shang, and Q. Wu, “Depth map enhancement by revisiting multi-scale intensity guidance within coarse-to-fine stages,” *IEEE Transactions on Circuits and Systems for Video Technology*, vol. 30, no. 12, pp. 4676–4687, 2019.
- [8] T.-W. Hui, C. C. Loy, and X. Tang, “Depth map super-resolution by deep multi-scale guidance,” in *European conference on computer vision*. Springer, 2016, pp. 353–369.
- [9] Z. Wang, X. Ye, B. Sun, J. Yang, R. Xu, and H. Li, “Depth upsampling based on deep edge-aware learning,” *Pattern Recognition*, vol. 103, p. 107274, 2020.
- [10] J. Tang, X. Chen, and G. Zeng, “Joint implicit image function for guided depth super-resolution,” in *Proceedings of the 29th ACM International Conference on Multimedia*, 2021, pp. 4390–4399.
- [11] Z. Zhong, X. Liu, J. Jiang, D. Zhao, Z. Chen, and X. Ji, “High-resolution depth maps imaging via attention-based hierarchical multi-modal fusion,” *IEEE Transactions on Image Processing*, vol. 31, pp. 648–663, 2021.
- [12] J. Ho, A. Jain, and P. Abbeel, “Denoising diffusion probabilistic models,” *Advances in neural information processing systems*, vol. 33, pp. 6840–6851, 2020.
- [13] J. Song, C. Meng, and S. Ermon, “Denoising diffusion implicit models,” *arXiv preprint arXiv:2010.02502*, 2020.
- [14] C. Saharia, J. Ho, W. Chan, T. Salimans, D. J. Fleet, and M. Norouzi, “Image super-resolution via iterative refinement,” *IEEE Transactions on Pattern Analysis and Machine Intelligence*, vol. 45, no. 4, pp. 4713–4726, 2022.
- [15] B. Xia, Y. Zhang, S. Wang, Y. Wang, X. Wu, Y. Tian, W. Yang, and L. Van Gool, “Diffir: Efficient diffusion model for image restoration,” *arXiv preprint arXiv:2303.09472*, 2023.
- [16] J. Liu, W. Zhang, Y. Tang, J. Qiao, and G. Wu, “Residual feature aggregation network for image super-resolution,” in *Proceedings of the IEEE/CVF conference on computer vision and pattern recognition*, 2020, pp. 2359–2368.
- [17] S. W. Zamir, A. Arora, S. Khan, M. Hayat, F. S. Khan, and M.-H. Yang, “Restormer: Efficient transformer for high-resolution image restoration,” in *Proceedings of the IEEE/CVF conference on computer vision and pattern recognition*, 2022, pp. 5728–5739.
- [18] H. Zhao, X. Kong, J. He, Y. Qiao, and C. Dong, “Efficient image super-resolution using pixel attention,” in *Computer Vision—ECCV 2020 Workshops: Glasgow, UK, August 23–28, 2020, Proceedings, Part III 16*. Springer, 2020, pp. 56–72.
- [19] N. Silberman, D. Hoiem, P. Kohli, and R. Fergus, “Indoor segmentation and support inference from rgb-d images,” in *Computer Vision—ECCV 2012: 12th European Conference on Computer Vision, Florence, Italy, October 7-13, 2012, Proceedings, Part V 12*. Springer, 2012, pp. 746–760.
- [20] H. Hirschmuller and D. Scharstein, “Evaluation of cost functions for stereo matching,” in *2007 IEEE conference on computer vision and pattern recognition*. IEEE, 2007, pp. 1–8.
- [21] D. Scharstein and C. Pal, “Learning conditional random fields for stereo,” in *2007 IEEE Conference on Computer Vision and Pattern Recognition*. IEEE, 2007, pp. 1–8.
- [22] S. Lu, X. Ren, and F. Liu, “Depth enhancement via low-rank matrix completion,” in *Proceedings of the IEEE conference on computer vision and pattern recognition*, 2014, pp. 3390–3397.
- [23] Y. Li, J.-B. Huang, N. Ahuja, and M.-H. Yang, “Deep joint image filtering,” in *Computer Vision—ECCV 2016: 14th European Conference, Amsterdam, The Netherlands, October 11–14, 2016, Proceedings, Part IV 14*. Springer, 2016, pp. 154–169.
- [24] S. Gu, W. Zuo, S. Guo, Y. Chen, C. Chen, and L. Zhang, “Learning dynamic guidance for depth image enhancement,” in *Proceedings of the IEEE conference on computer vision and pattern recognition*, 2017, pp. 3769–3778.
- [25] Y. Li, J.-B. Huang, N. Ahuja, and M.-H. Yang, “Joint image filtering with deep convolutional networks,” *IEEE transactions on pattern analysis and machine intelligence*, vol. 41, no. 8, pp. 1909–1923, 2019.
- [26] X. Deng and P. L. Dragotti, “Deep convolutional neural network for multi-modal image restoration and fusion,” *IEEE transactions on pattern analysis and machine intelligence*, vol. 43, no. 10, pp. 3333–3348, 2020.
- [27] B. Kim, J. Ponce, and B. Ham, “Deformable kernel networks for joint image filtering,” *International Journal of Computer Vision*, vol. 129, no. 2, pp. 579–600, 2021.
- [28] Z. Zhao, J. Zhang, S. Xu, Z. Lin, and H. Pfister, “Discrete cosine transform network for guided depth map super-resolution,” in *Proceedings of the IEEE/CVF Conference on Computer Vision and Pattern Recognition*, 2022, pp. 5697–5707.